Geophysical Research Letters

RESEARCH LETTER
10.1029/2018GL081332

Quantifying the Role of Oceanic Feedbacks on ENSO Asymmetry

Cong Guan[1,2,3,4,5], **Michael J. McPhaden**[6], **Fan Wang**[1,2,4,5], **and Shijian Hu**[1,2,4,5]

[1]Key Laboratory of Ocean Circulation and Waves, Institute of Oceanology, Chinese Academy of Sciences, Qingdao, China, [2]College of Marine Science, University of Chinese Academy of Sciences, Qingdao, China, [3]Institute of Oceanographic Instrumentation, Shandong Academy of Sciences, Qingdao, China, [4]Center for Ocean Mega-Science, Chinese Academy of Sciences, Qingdao, China, [5]Qingdao National Laboratory for Marine Science and Technology, Qingdao, China, [6]NOAA/Pacific Marine Environmental Laboratory, Seattle, WA, USA

Abstract The role of oceanic feedbacks in determining the asymmetry of El Niño–Southern Oscillation (ENSO) magnitude, spatial structure, and duration is quantified on the basis of a novel temperature variance budget. Results confirm previous studies that in the eastern Pacific, El Niño warm temperature anomalies are larger in magnitude than La Niña cold temperature anomalies mainly due to stronger positive oceanic feedbacks for El Niño. We find that La Niña cold anomalies are typically stronger than El Niño warm anomalies in the central Pacific with a faster growth rate for cold anomalies, due to a stronger positive thermocline feedback and weaker nonlinear damping. The thermocline feedback related to recharge oscillator dynamics plays a dominate role and leads to asymmetry in the duration of El Niño and La Niña events. In particular, the thermocline feedback becomes significantly negative during the late decaying phase of El Niño and speeds up its demise.

Plain Language Summary The El Niño–Southern Oscillation (ENSO) is well known to have profound impacts on global climate. Many asymmetric features exist between its warm phase of ENSO (El Niño) and cold phase (La Niña), but their causes are still not fully understood. Our study examines three aspects of ENSO asymmetry: (1) the amplitude of anomalous temperature during the mature El Niño events is larger than La Niña in the equatorial eastern Pacific; (2) in the equatorial central Pacific, the amplitude in mature phase of La Niña is larger than El Niño; and 3) La Niña typically lasts longer than El Niño events. We find that the larger amplitude of El Niño than La Niña is due to stronger positive feedback for El Niño in the eastern Pacific. In the central Pacific, La Niña has a faster growth rate than El Niño, which may be induced by stronger positive thermocline feedback in the developing phase and less nonlinear damping effect. The asymmetry of ENSO duration is because the decay rate for La Niña events is slower than for El Niño, as a result of positive thermocline feedback that change sign to negative for El Niño but not for La Niña.

Key Points:
- El Niño is stronger than La Niña in the eastern Pacific due to stronger positive feedbacks during El Niño events
- La Niña is stronger than El Niño in the central Pacific because the thermocline feedback is stronger and reinforced by nonlinearity
- Asymmetry in El Niño-La Niña duration results from asymmetric thermocline feedback related to the recharge oscillator dynamics

Supporting Information:
- Supporting Information S1

Correspondence to:
C. Guan,
congguan@qdio.ac.cn

Citation:
Guan, C., McPhaden, M. J., Wang, F., & Hu, S. (2019). Quantifying the role of oceanic feedbacks on ENSO asymmetry. *Geophysical Research Letters*, *46*, 2140–2148. https://doi.org/10.1029/2018GL081332

Received 26 NOV 2018
Accepted 9 JAN 2019
Accepted article online 15 JAN 2019
Published online 18 FEB 2019

1. Introduction

The El Niño–Southern Oscillation (ENSO) is the most prominent interannual phenomenon on the planet, impacting climate patterns and their variability worldwide (McPhaden et al., 2006). Its warm phase, known as El Niño, occurs with warm sea surface temperature (SST) anomalies in the equatorial Pacific accompanied by weakened trade winds along the equator, while the converse holds true for its cold phase, La Niña. A delicate balance of positive and negative feedbacks controls El Niño and La Niña events by either amplifying or damping ENSO anomalies. Key positive feedbacks that determine the growth rate of ENSO events include the thermocline feedback (TCF) due to effects of wind-driven equatorial thermocline depth variations on SST, the Ekman feedback (EKF) that results from anomalous vertical advection of temperature driven by local winds, and the zonal advective feedback (ZAF) associated with anomalous thermal advection by zonal currents (e.g., Jin et al., 2006). Net sea surface heat flux typically acts as the largest negative feedback that damps SST anomalies (e.g., Zhang & McPhaden, 2010).

El Niño and La Niña are like two sides of one coin, but they are not exactly symmetrical and exhibit significant complexity (Timmermann et al., 2018). It is well known that the magnitude of El Niño SST anomalies is usually greater than for La Niña, as evident by stronger warm SST anomalies than negative anomalies in the

eastern Pacific (EP; Deser & Wallace, 1987). The spatial distribution of El Niño SST anomalies is also clearly asymmetrical with La Niña anomalous SST pattern shifted to the west compared to El Niño (Dommenget et al., 2013; Hoerling et al., 1980). Significant differences also exist in the duration and phase transitions of El Niño and La Niña (Choi et al., 2013; DiNezio & Deser, 2014; Dommenget et al., 2013; Kug & Ham, 2011; Larkin & Harrison, 2002; McGregor et al., 2013; Okumura & Deser, 2010). For example, El Niño events generally decay by the summer following their mature phase, but La Niña events often persist through a second year (Santoso et al., 2017). The frequent occurrence of a second-year La Niña is a notable departure from a purely linear ENSO cycle (Kessler, 2002). These asymmetric features between El Niño and La Niña can project onto decadal or even longer time scale variability in the tropical Pacific Ocean (An, 2004; Monahan & Dai, 2004; Rodgers et al., 2004).

Several hypotheses have been proposed to understand ENSO asymmetry. Some studies have shown that a nonlinear relationship between SST and zonal wind stress can contribute to the El Niño-La Niña asymmetry (e.g., Frauen & Dommenget, 2010). Jin et al. (2003) pointed out that the vertical nonlinear thermal advection plays a role in affecting amplitude asymmetry between El Niño and La Niña. Wang and McPhaden (2001) found that anomalous vertical mixing at the base of ocean mixed layer enhances warm El Niño SSTs while the tropical instability waves in the EP weaken cold La Niña SSTs. Su et al. (2010) also argued that nonlinear horizontal thermal advection contributes to the asymmetry between El Niño and La Niña. For the same magnitude of warm water volume anomaly in the equatorial Pacific, Meinen and McPhaden (2000) found that positive El Niño SST anomalies were much greater than negative La Niña SST anomalies though they could only speculate as to the reasons. Im et al. (2015) used Bjerknes stability index and pointed out that stronger positive feedbacks contribute to a larger growth rate in the El Niño phase. However, the Bjerknes index is by definition limited to describing impacts on EP SSTs and might overestimate TCF relative to ZAF (Graham et al., 2014). Recent studies also emphasized the importance of ZAF on amplitude asymmetry of ENSO (Kim et al., 2015; Santoso et al., 2017). It has been suggested that equatorial zonal transport (Chen et al., 2016) and the meridional gradient of sea surface height anomalies (Hu et al., 2016) affect the asymmetry of El Niño and La Niña decay phases, but precisely, how much these oceanic processes contribute to El Niño-La Niña asymmetry is still unanswered.

In this study, we apply a novel temperature variance budget approach as used in Guan and McPhaden (2016, hereafter GM2016) to quantitatively estimate the role of various oceanic feedbacks in affecting the asymmetry of ENSO with respect of amplitude, spatial structure, and event duration. Compared to a traditional temperature budget analysis, the temperature variance budget can be used to estimate how different processes contribute to the temperature variance growth or decay and to explicitly identify which terms are positive feedbacks (creating variance) and which are negative feedback (damping variance). The temperature variance budget and data we use are described in section 2. Main results are presented in section 3 followed in section 4 by a summary and discussion of outstanding issues.

2. Temperature Variance Budget and Data

To examine individual oceanic feedbacks in a unified framework, we make use of a temperature variance budget developed by Santoso et al. (2010) and elaborated on in GM2016. The governing equation is constructed by multiplying the temperature equation by temperature anomalies:

$$\mathrm{MLT}^{\nu}{}_{t} = \mathrm{TCF} + \mathrm{EKF} + \mathrm{ZAF} + \mathrm{MAF} + \mathrm{MHD} + \mathrm{TD} + \mathrm{NL} + \mathrm{R}, \tag{1}$$

where $\mathrm{MLT}^{\nu}{}_{t}$ is the time-dependent temperature variance tendency and on right-hand side are shown as the feedback terms TCF, EKF, ZAF, meridional advective feedback, mean horizontal dynamical heating term (MHD), thermal damping by net sea surface heat flux (TD), and nonlinear advection, respectively. The residual R represents the difference between $\mathrm{MLT}^{\nu}{}_{t}$and the sum of the seven feedbacks. This residual contains computational errors, the effects of unresolved physical processes such as vertical heat diffusion, tropical instability waves not represented explicitly the monthly products used, and penetrative shortwave radiation, which cannot be computed from net surface heat flux provided by the reanalysis products. In addition, since we use reanalysis products to evaluate (1), the residual will also contain assimilation increments from the various products (as discussed in GM2016). Detailed formulas and specific definitions for the temperature variance budget are provided in the appendix and also described in GM2016.

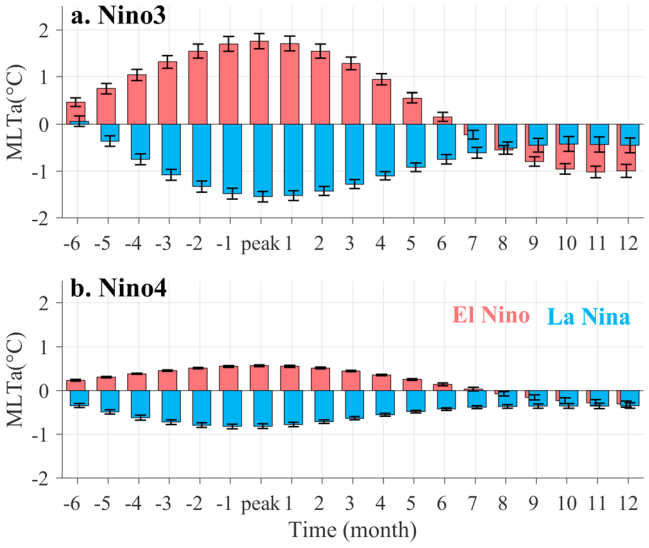

Figure 1. Ensemble mean mixed layer temperature (MLT) anomalies for composite El Niño–Southern Oscillation (ENSO) events in (a) Niño3 and (b) Niño4 regions. El Niño events are shown in red, and La Niña in blue. The *x* axis represents time in months, with negative values being months before the peak of ENSO events, and positive values being months after the peak. Error bars are 95% confidence levels from all the corresponding ENSO events across the four model products.

We use three ocean reanalysis products and one numerical ocean general circulation model simulation for budget calculations. These include the German Estimating the Circulation and Climate of the Ocean Version 2 (GECCO2; Köhl & Stammer, 2008) from Hamburg University, the ocean analysis/reanalysis system version 3 (ORAS3; Balmaseda et al., 2008) and version 4 (ORAS4; Balmaseda et al., 2013) provided by the European Centre for Medium-Range Weather Forecasts and also the ocean general circulation model of the Earth Simulator (Masumoto et al., 2004) based on the MOM3. Detailed description of these four model products can be found from the Asia-Pacific Data-Research Center at the University of Hawaii (http://apdrc.soest.hawaii.edu/data/data.php). Budget calculations are based on the monthly fields of ocean current velocities, ocean temperature, and net sea surface heat flux (q_{net}) from these four products. Vertical velocity and surface heat flux are not available for ORAS4, so for this product we calculated vertical velocities based on mass continuity and used surface heat fluxes from the ERA-interim reanalysis. Periods cover from January 1980 to December 2010. To obtain the interannual signals of each feedback, we used Fourier low-pass filter with a cutoff period of 15 months (Walters & Heston, 1982). Budget calculations are carried out using the method described in Lee et al. (2004) within a 50-m mixed layer of both the Niño3 region (5°S to 5°N, 150–90°W) and Niño4 region (5°S to 5°N, 160°E to 150°W) for each product then averaged to provide an ensemble mean perspective. All these four products present reasonable good closure of heat balance (refer to Figure 3 in GM2016).

Niño3 and Niño4 indices are used to represent ENSO SST anomalies in the EP and central Pacific (CP), respectively. These two index regions are helpful in characterizing CP/EP El Niño events (e.g., Kug et al., 2009) and ENSO diversity (e.g., Santoso et al., 2017). Here we defined the indices based on interannual anomalies of mixed layer temperature (MLT) in the corresponding Niño regions and then defined an event when the index is over 0.5 °C for El Niño or below −0.5 °C for La Niña for 6 months or more. As a result, nine El Niño and six La Niña events are identified in the Niño3 region, while nine El Niño and four La Niña events are identified in the Niño4 region (see details in Table S1 in the supporting information). Then general composite analysis is deployed separately for El Niño and La Niña in each Niño region, with events centered at their peaks determined as the month of maximum ENSO MLT anomaly. We tried different ways to characterize ENSO events such as selecting events with the criterion of 0.5 °C thresholds for both regions simultaneously or using a threshold of 1 °C. Either of these options reduces the number of events in our ensemble and therefore increases uncertainties. Also, 0.5 °C is a widely accepted criterion for identifying ENSO events, so we chose to use this criterion to select ENSO events separately in each region.

To estimate uncertainty, we treated each El Niño and La Niña event of each reanalysis product as separate realizations. Thus, we have 36 realizations of El Niño in the Niño3 and Niño4 regions, 24 realizations of La Niña in the Niño3 region, and 16 realizations in the Niño4 region. We then computed standard error and 95% confidence limits considering each event to be independent in its respective index region. These 95% confidence limits are shown as error bars in Figures 1–3.

3. Results

The asymmetry in ENSO evolution is characterized in the composite ENSO MLT anomalies (Figure 1). It is evident that El Niño has a larger amplitude than La Niña in the Niño3 region (Figure 1a), but the situation is reversed in the Niño4 region (Figure 1b). The difference of ENSO amplitude between the Niño3 and Niño4 regions also indicates clear asymmetry in spatial structure. La Niña also tends to last longer than El Niño, especially during respective decaying phases in the Niño3 region (Figures 1a and S1). On average, an El Niño event quickly declines after its peak and returns to a neutral state within 6 months. Conversely, La Niña decays much more slowly with negative MLT anomalies still exceeding 0.8 °C 6 months after its peak, sometimes even followed by a weak second-year cold event.

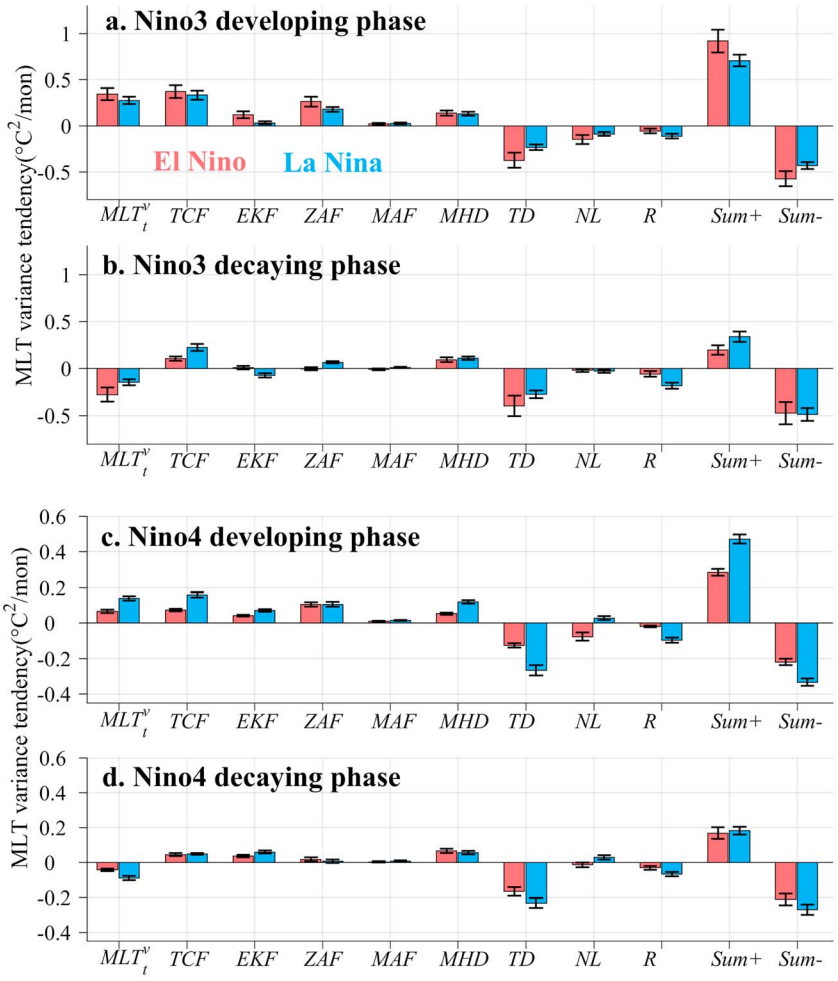

Figure 2. Individual terms from the temperature variance budget averaged among the developing phase (a, c) and decaying phase (b, d) in the Niño3 and Niño4 regions, respectively. Sum of the five positive feedbacks, for example, TCF, EKF, ZAF, MAF, and MHD, is shown as Sum+, and sum of the three negative feedbacks, for example, TD, NL, and the residual R, is shown as Sum−. Error bars are 95% confidence levels from all the corresponding El Niño–Southern Oscillation events across the four model products. MLT = mixed layer temperature; TCF = thermocline feedback; EKF = Ekman feedback; ZAF = zonal advective feedback; MAF = meridional advective feedback; MHD = mean horizontal dynamical heating term; NL = nonlinear; TD = thermal damping; R = residual.

To evaluate roles of various oceanic feedbacks in controlling these ENSO MLT asymmetries, we analyzed the temperature variance budget for El Niño and La Niña events separately in the Niño3 and Niño4 regions. Then averages of each budget term are made over the 6 months before the ENSO peak (i.e., ENSO developing phase) and 6 months after (i.e., ENSO decaying phase). In general, TCF and ZAF are the largest two positive feedbacks causing El Niño and La Niña temperature anomalies to grow in both Niño3 and Niño4 regions. During the decay phase in both regions, TCF is reduced but still on average positive while ZAF is nearly to 0 on average (Figure 2). EKF and MHD are typically weaker positive feedbacks particularly during the development phase. Regarding negative feedbacks, TD is clearly the largest negative term in both developing and decaying phases in the both regions. These results are consistent with previous studies (e.g., GM2016; Kug et al., 2009; Ren & Jin, 2013; Zhang & McPhaden, 2010) though there are some differences as well. We find that the nonlinear feedback, for example, is generally negative according to our formalism, while it is positive for warm ENSO events according to Jin et al. (2003). This discrepancy may result from the particular regions chosen for analysis and also the particular choice of product (GM2016). The residual R manifests itself as a negative feedback.

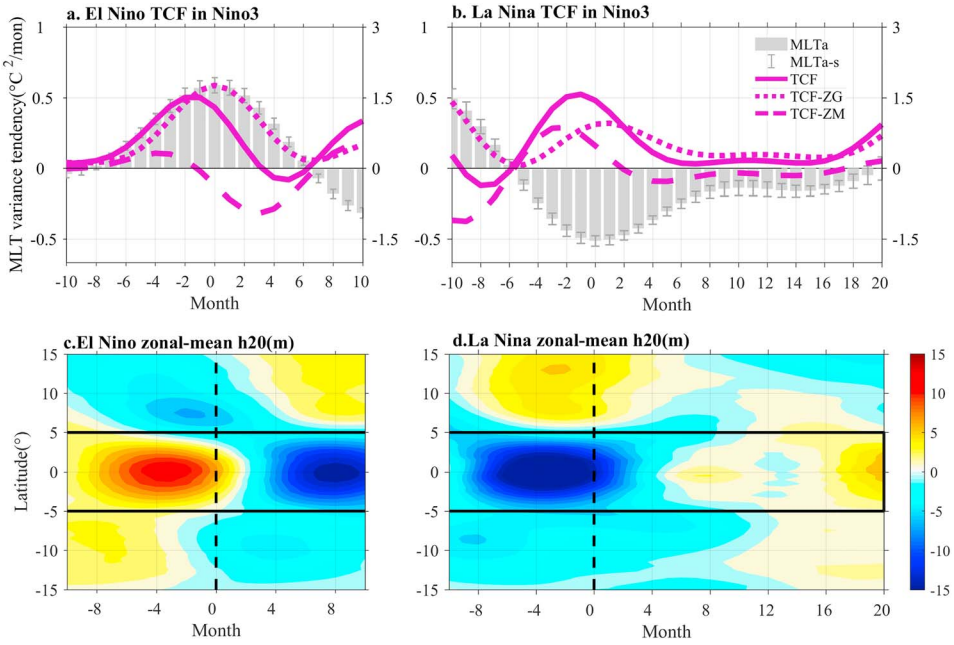

Figure 3. TCF components superimposed on MLT variations (a, b) and thermocline depth averaged across the Pacific basin (c, d) during the composite El Niño (a, c) and La Niña (b, d). Thick black dashed lines in (c) and (d) present the peak months of ENSO event development. Error bars in (a) and (b) are 95% confidence levels from all the corresponding ENSO events across the four model products. ENSO = El Niño–Southern Oscillation; MLT = mixed layer temperature; TCF = thermocline feedback; ZG = zonal gradient; ZM = zonal mean.

We next compare each of the oceanic feedbacks between El Niño and La Niña to better understand their roles in generating ENSO asymmetries. In the Niño3 region, El Niño has a greater growth rate than La Niña, which is attributed to stronger positive feedbacks during El Niño (Figure 2a). To quantify the relative contribution of each positive feedback, the percentage ratio is calculated as the El Niño-La Niña difference in each positive feedback divided by the difference in total positive feedbacks (shown as Sum+ in Figure 2) between El Niño and La Niña. Among the positive feedbacks, the biggest El Niño-La Niña difference in positive feedbacks is for ZAF, EKF, and TCF, which contribute 36%, 33%, and 25% to the difference in total positive feedbacks, respectively. Together, they can explain 94% of the total difference in positive feedbacks, among which the difference in ZAF is the largest. The sum of the negative feedbacks also shows significant El Niño-La Niña difference. This difference comes mainly from the difference in TD, which damps temperature anomalies once developed. Nonlinear feedback, as a damping term, is also stronger in El Niño than La Niña. Therefore, stronger positive oceanic feedbacks during El Niño, especially the stronger ZAF, EKF and TCF, account for larger El Niño than La Niña amplitudes in the EP. Im et al. (2015) also attributed ENSO amplitude asymmetry to these three feedbacks but arrived at a different relative ranking of ZAF > TCF > EKF based on a Bjerknes index analysis. We note that the percentages for these three positive feedbacks in our analysis are not significantly different from one another in a statistical sense and that relative rankings may be sensitive to different products or methods used (Graham et al., 2014).

In the Niño4 region, the growth rate of the La Niña is stronger than that of El Niño, due to stronger positive feedbacks for La Niña events (Figure 2c). Among the positive oceanic feedbacks, the TCF shows a prominent difference and contributes about 46% of the difference in total positive feedbacks. The MHD contributes the secondarily (36%), followed by EKF (16%). It is interesting that though ZAF is suggested to be the dominant positive feedback controlling the CP ENSO events (Guan et al., 2013), there is no significant difference in ZAF between El Niño and La Niña events in this region. Regarding the negative feedbacks, TD shows a significant difference between El Niño and La Niña, but with a larger uncertainty for La Niña from the four model products. We note that nonlinearity acts as a negative feedback in El Niño but is a positive feedback in La Niña. The residual R also exhibits a notable El Niño-La Niña difference but also shows relatively high uncertainty. Thus, we suggest the larger growth rate for La Niña than El Niño in Niño4 is due to stronger positive TCF reinforced (rather than opposed) by nonlinear effect.

We note that the composite growth rates for El Niño and La Niña in the Niño3 region are not as asymmetric as in the Niño4 region statistically. Santoso et al. (2017) noted that some strong La Niñas, such as in 1998–1999, were preconditioned by very warm El Niño SSTs, which required very strong positive feedbacks to flip warm condition to cold. Thus, from our composite analysis, the El Niño-La Niña asymmetry tends to be weak in the Niño3 region. In contrast, the Niño4 region exhibits much stronger asymmetry, perhaps because we identified events separately for each region.

The asymmetry in El Niño-La Niña duration is mainly determined by differences in the decaying phase, which is significant in the Niño3 region (Figure 1a), where La Niña has an obviously slower decay rate than El Niño (Figure 2b). This asymmetry is caused by the sum of positive feedbacks in the decaying phase of La Niña being much larger than for El Niño. Among these feedbacks, the positive TCF shows the biggest difference, being twice as large for La Niña than El Niño. Difference can be also found in the ZAF, which though small is also positive for La Niña but essentially 0 for El Niño. In fact, the TCF and ZAF feedbacks actually become negative for period during the late decaying phase of El Niños (Figure S1), especially during strong EP events (GM2016). In contrast, this tendency for TCF and ZAF to become negative during the decay phase of La Niña events is not evident (Figure S1b). Thus on average, these feedbacks, especially TCF, are still actively opposing the damping processes that would otherwise terminate La Niña events more quickly. In the Niño4 region, La Niña also tends to decay more slowly than El Niño (Figures 1b and S2) but with a larger decay rate than El Niño (Figure 2d). Unlike in Niño3, however, the differences in most feedbacks between El Niño and La Niña are not significant, except for larger damping effects of negative TD and R in La Niña events. This likely results from the initial condition (Santoso et al., 2017) that the negative SST anomalies in the Niño4 region are much stronger than positive anomalies at their peaks, so that these negative feedbacks are not sufficient to terminate cold anomalies in this region.

We find that the TCF is a major process affecting the growth and decay of ENSO events and their asymmetries. Based on model simulations of a nonlinear delayed oscillator, DiNezio and Deser (2014) also found that delayed TCF contributed to the multiyear persistence of La Niña events vis a vis El Niño events. Thus, we will next examine in detail how the TCF related to recharge oscillator dynamics affects the asymmetric decay of ENSO events in the Niño3 region.

The TCF affects both the growth rates and phase transition of ENSO events according to Jin's (1997) recharge oscillator theory, through the anomalous zonal gradient and zonal mean of the thermocline depth across the Pacific basin, respectively. To further investigate the role of TCF in the asymmetric duration of El Niño and La Niña, we first separate the anomalies in thermocline depth (defined as 20 °C isotherm depth, i.e., $h20$) in the Niño3 region into two parts following GM2016 as $h20_{\mathrm{nino3}} = h20_{\mathrm{ZG}} + h20_{\mathrm{ZM}}$, where the subscripted ZG and ZM represent for zonal gradient and zonal mean of the variable, respectively. Since the vertical temperature difference at the bottom of the mixed layer, which determines the TCF, is highly correlated and in phase with the $h20_{\mathrm{Niño3}}$, we thus further separate the TCF into two parts, that is, $\mathrm{TCF} = \mathrm{TCF}_{\mathrm{ZG}} + \mathrm{TCF}_{\mathrm{ZM}}$(details can be found in GM2016). In Figures 3a and 3b, the TCF induced by zonal gradient of thermocline variations ($\mathrm{TCF}_{\mathrm{ZG}}$) always acts as a positive feedback throughout both warm and cold ENSO events, while TCF caused by zonal mean thermocline variations ($\mathrm{TCF}_{\mathrm{ZM}}$) acts as positive feedback during the developing phase and negative feedback during the decaying phase. To compare the differences between El Niño and La Niña, the positive $\mathrm{TCF}_{\mathrm{ZG}}$ in the decaying phase is relatively small for La Niña. However, $\mathrm{TCF}_{\mathrm{ZM}}$ is 3 times larger as a negative feedback (−0.3 °C/month) during the decaying phase of El Niño than that of La Niña (−0.1 °C/month). Thus, the relatively strong negative $\mathrm{TCF}_{\mathrm{ZM}}$during the decaying phase of El Niño helps to accelerate the demise of warm events but not so much cold events. From Figures 3c and 3d it is evident that the zonal mean thermocline quickly shoals after El Niño peaks, whereas during La Niña the corresponding deepening is very gradual. Therefore, we conclude that the El Niño-La Niña difference in TCF during their respective decay phases results from asymmetric changes in zonal mean thermocline depth across the equatorial Pacific, indicating an asymmetry in underlying recharge oscillator dynamics.

4. Summary and Discussion

In this paper, the El Niño-La Niña SST asymmetries in respect of magnitude, spatial distribution, and duration are interpreted from a perspective of oceanic feedbacks, based on a temperature variance analysis in the Niño3 and Niño4 regions. We use a composite analysis to look for common characteristics

across all warm and cold events and find that composite El Niño events are stronger than La Niña events in the Niño3 region due primarily to stronger positive feedbacks and in particular stronger ZAF, EKF, and TCF. In the Niño4 region, however, La Niña has a faster growth rate and thus is stronger than El Niño. The difference in growth rates is mainly due to the differences in positive feedbacks, among which TCF is most prominent followed by MHD and EKF. Nonlinear processes reinforce these positive feedbacks during La Niña but oppose them during El Niño, which also contributes to the faster development of La Niña. Therefore, our results are consistent with previous studies (e.g., Choi et al., 2013; Im et al., 2015) that positive oceanic feedbacks lead to asymmetries in El Niño-La Niña amplitude in the Niño3 region but also determined with more precise localization that TCF and nonlinear damping result in asymmetrical growth rate in the Niño4 region.

Asymmetry in El Niño-La Niña duration comes mainly from their decaying phases, with a larger decay rate found for El Niño than La Niña. The TCF shows the largest difference among the positive feedbacks and thus contributes to this difference in decay rates. Guided by recharge oscillator theory, we separate TCF affects into two parts: TCF_{ZG} caused by zonal gradient thermocline variations and TCF_{ZM} caused by zonal mean thermocline variations. During the decay phase of El Niño in the equatorial EP, TCF_{ZM} acts as a prominent negative feedback as large as −0.3 °C/month, which is at least three times stronger than during the decaying phase of La Niña (only −0.1 °C/month at most). This difference is induced by zonal mean thermocline changes, which quickly shoals across the equator after El Niño peaks, whereas a very slow deepening occurs during the decaying phase of La Niña. Therefore, ENSO asymmetry in duration results from an underlying asymmetry in recharge oscillator dynamics. This result is consistent with Kessler (2002), who stated that the recharge process is weak after the peak of La Niña events before the onset of another El Niño.

What causes the asymmetry of recharge processes during the ENSO decaying phases? A recent study by Neske and McGregor (2018) attributes this asymmetry to an asymmetry in oceanic processes, with the discharged phase of the cycle dominated by the adjusted wave dynamics and the recharged phase dominated by the instantaneous wind-induced Ekman mass transport. Hu et al. (2016), on the other hand, speculated the convergence of anomalous meridional currents from the off-equatorial oceans onto the equator may help to slow down the recharge process during the decaying phase of La Niña. From the anomalous wind stress pattern averaged during the decaying phase of a composite La Niña event (Figure S3b), anomalous eastward wind stress and negative wind curl are found in the EP, which may drive the convergence of anomalous meridional currents suggested by Hu et al. (2016). Also we note that the asymmetry of wind stress pattern (Figure S3c) looks very similar to the asymmetric wind stress from McGregor et al. (2013), implying the asymmetry in recharge oscillator dynamics is also related to asymmetries in the surface winds.

In the present study we have quantitatively examined various oceanic processes affecting the El Niño-La Niña asymmetry. Our results confirm previous studies about the role of TCFs related to recharge oscillator dynamics in determining the asymmetry in El Niño-La Niña duration and provide robust evidence from the perspective of a detailed temperature variance budget analysis for the first time. However, recent studies show that the recharge oscillator dynamics is a less effective determinant of ENSO variability after the year 2000 (e.g., GM2016; McPhaden, 2012; Neske & McGregor; 2018), related to the more frequent occurrence of CP El Niño events (Lee & McPhaden, 2010; Wen et al., 2014; Xiang et al., 2013). In addition, accounting for the slowdown in global warming between about 2000 and 2013, the Pacific trade winds significantly strengthened and an increase in subsurface ocean heat uptake was found in the equatorial thermocline (e.g., England et al., 2014). How asymmetries in the ENSO cycle are manifest for different flavors of El Niño and La Niña and under changing background conditions are the subject of a future study.

Appendix A.

Temperature variance budget (equation (1)) written in terms of individual feedback terms:

$$\mathrm{MLT}_t^{\nu} = \mathrm{TCF} + \mathrm{EKF} + \mathrm{ZAF} + \mathrm{MAF} + \mathrm{MHD} + \mathrm{TD} + \mathrm{NL} + \mathrm{R}$$

where

$$\mathrm{MLT}_t^{\nu} = \frac{1}{2}\partial(T_{\mathrm{ave}}')^2/\partial \mathrm{t} = \frac{1}{2}(\mathrm{MLT}^{\nu})_{\mathrm{t}}$$

$$\mathrm{TCF} = \frac{1}{B}\iint \overline{w_B}\delta T_B' \cdot T_{\mathrm{ave}}' \mathrm{d}x\mathrm{d}y$$

$$\mathrm{EKF} = \frac{1}{B}\iint w_B' \overline{\delta T_B} \cdot T_{\mathrm{ave}}' \mathrm{d}x\mathrm{d}y$$

$$\mathrm{ZAF} = \frac{1}{B}\iint \left(u_W' \overline{\delta T_W} - u_E' \overline{\delta T_E}\right) \cdot T_{\mathrm{ave}}' \mathrm{d}y\mathrm{d}z$$

$$\mathrm{MAF} = \frac{1}{B}\iint \left(v_S' \overline{\delta T_S} - v_N' \overline{\delta T_N}\right) \cdot T_{\mathrm{ave}}' \mathrm{d}x\mathrm{d}z$$

$$\mathrm{MHD} = \frac{1}{B}\left[\iint (\overline{u_W}\delta T_W' - \overline{u_E}\delta T_E') \cdot T_{\mathrm{ave}}' \mathrm{d}y\mathrm{d}z + \iint (\overline{v_S}\delta T_S' - \overline{v_N}\delta T_N') \cdot T_{\mathrm{ave}}' \mathrm{d}x\mathrm{d}z\right]$$

$$\mathrm{NL} = \frac{1}{B}\left[\begin{array}{l} \iint (u_W'\delta T_W' - u_E'\delta T_E') \cdot T_{\mathrm{ave}}' \mathrm{d}y\mathrm{d}z + \iint \left(v_S'\delta T_S' - v_N'\delta T_N'\right) \cdot T_{\mathrm{ave}}' \mathrm{d}x\mathrm{d}z \\ + \iint w_B'\delta T_B' \cdot T_{\mathrm{ave}}' \mathrm{d}x\mathrm{d}y \end{array}\right]$$

$$\mathrm{TD} = \frac{1}{\rho c_p B}\iint q_{\mathrm{net}}' \cdot T_{\mathrm{ave}}' \mathrm{d}x\mathrm{d}y$$

Acknowledgments

We thank three anonymous reviewers for their constructive comments on the original version of this manuscript. We acknowledge Hamburg University, JAMSTEC APL, and ECMWF for their valuable reanalysis and model products. This study was supported by the National Natural Science Foundation of China (Grants 41806016 and 41730534), the China Postdoctoral Science Foundation (2017M622289), Qingdao postdoctoral application research project, the National Natural Science Foundation of China (Grant 41776018), the National Program on Global Change and Air-Sea Interaction (GASI-IPOVAI-01-01), and the Key Research Program of Frontier Sciences, CAS (QYZDB-SSW-SYS023). PMEL contribution number is 4814. The four model products data are available from the Asia-Pacific Data-Research Center at the University of Hawaii (http://apdrc.soest.hawaii.edu/data/data.php).

References

An, S.-I. (2004). Interdecadal changes in the El Niño–La Niña asymmetry. *Geophysical Research Letters*, *31*, L23210. https://doi.org/10.1029/2004GL021699

Balmaseda, M. A., Mogensen, K., & Weaver, A. T. (2013). Evaluation of the ECMWF ocean reanalysis system ORAS4. *Quarterly Journal of the Royal Meteorological Society*, *139*(674), 1132–1161. https://doi.org/10.1002/qj.2063

Balmaseda, M. A., Vidard, A., & Anderson, D. L. T. (2008). The ECMWF ocean analysis system: ORA-S3. *Monthly Weather Review*, *136*(8), 3018–3034. https://doi.org/10.1175/2008MWR2433.1

Chen, H. C., Hu, Z. Z., Huang, B., & Sui, C. H. (2016). The role of reversed equatorial zonal transport in terminating an ENSO event. *Journal of Climate*, *29*(16), 5859–5877. https://doi.org/10.1175/JCLI-D-16-0047.1

Choi, K. Y., Vecchi, G. A., & Wittenberg, A. T. (2013). ENSO transition, duration, and amplitude asymmetries: Role of the nonlinear wind stress coupling in a conceptual model. *Journal of Climate*, *26*(23), 9462–9476. https://doi.org/10.1175/JCLI-D-13-00045.1

Deser, C., & Wallace, J. M. (1987). El Niño events and their relation to the southern oscillation: 1925–1986[J]. *Journal of Geophysical Research*, *92*(C13), 14,189–14,196. https://doi.org/10.1029/JC092iC13p14189

DiNezio, P. N., & Deser, C. (2014). Nonlinear controls on the persistence of La Niña. *Journal of Climate*, *27*(19), 7335–7355. https://doi.org/10.1175/JCLI-D-14-00033.1

Dommenget, D., Bayr, T., & Frauen, C. (2013). Analysis of the non-linearity in the pattern and time evolution of El Niño southern oscillation. *Climate Dynamics*, *40*(11–12), 2825–2847. https://doi.org/10.1007/s00382-012-1475-0

England, M. H., McGregor, S., Spence, P., Meehl, G. A., Timmermann, A., Cai, W., et al. (2014). Recent intensification of wind-driven circulation in the Pacific and the ongoing warming hiatus. *Nature Climate Change*, *4*(3), 222–227. https://doi.org/10.1038/nclimate2106

Frauen, C., & Dommenget, D. (2010). El Niño and La Niña amplitude asymmetry caused by atmospheric feedbacks. *Geophysical Research Letters*, *37*, L18801. https://doi.org/10.1029/2010GL044444

Graham, F. S., Brown, J. N., Langlais, C., Marsland, S. J., Wittenberg, A. T., & Holbrook, N. J. (2014). Effectiveness of the Bjerknes stability index in representing ocean dynamics. *Climate Dynamics*, *43*(9-10), 2399–2414. https://doi.org/10.1007/s00382-014-2062-3

Guan, C., Chen, Y.-L., & Wang, F. (2013). Seasonal variability of zonal heat advection in the mixed layer of the tropical Pacific. *Chinese Journal of Oceanology and Limnology*, *31*(6), 1356–1367. https://doi.org/10.1007/s00343-014-3019-4

Guan, C., & McPhaden, M. J. (2016). Ocean processes affecting the twenty-first-century shift in ENSO SST variability. *Journal of Climate*, *29*(19), 6861–6879. https://doi.org/10.1175/JCLI-D-15-0870.1

Hoerling, M. P., Kumar, A., & Zhong, M. (1980). El Niño, La Niña, and the nonlinearity of their teleconnections. *Journal of Climate*, *10*(10), 1769–1786.

Hu, Z. Z., Kumar, A., Huang, B., Zhu, J., Zhang, R.-H., & Jin, F.-F. (2016). Asymmetric evolution of El Niño and La Niña: The recharge/discharge processes and role of the off-equatorial sea surface height anomaly. *Climate Dynamics*, *49*(7–8), 1–12.

Im, S., An, S.-I., Kim, S. T., & Jin, F.-F. (2015). Feedback processes responsible for El Niño-La Niña amplitude asymmetry. *Geophysical Research Letters*, *42*, 5556–5563. https://doi.org/10.1002/2015GL064853

Jin, F. F. (1997). An equatorial ocean recharge paradigm for ENSO. Part I: Conceptual model.[J]. *Journal of the Atmospheric Sciences*, *54*(7), 811–829. https://doi.org/10.1175/1520-0469(1997)054<0811:AEORPF>2.0.CO;2

Jin, F. -F., An, S. I., Timmermann, A., & Zhao, J. (2003). Strong El Niño events and nonlinear dynamical heating. *Geophysical Research Letters*, *30*(3), 1120. https://doi.org/10.1029/2002GL016356

Jin, F.-F., Kim, S. T., & Bejarano, L. (2006). A coupled-stability index for ENSO. *Geophysical Research Letters*, *33*, L23708. https://doi.org/10.1029/2006GL027221

Kessler, W. S. (2002). Is ENSO a cycle or a series of events? *Geophysical Research Letters*, *29*(23), 2125. https://doi.org/10.1029/2002GL015924

Kim, W., Cai, W., & Kug, J.-S. (2015). Migration of atmospheric convection coupled with ocean currents pushes El Niño to extremes. *Geophysical Research Letters*, *42*, 3583–3590. https://doi.org/10.1002/2015GL063886

Köhl, A., & Stammer, D. (2008). Variability of the meridional overturning in the North Atlantic from the 50-yr GECCO state estimation. *Journal of Physical Oceanography*, *38*(9), 1913–1930. https://doi.org/10.1175/2008JPO3775.1

Kug, J., & Ham, Y. (2011). Are there two types of La Niña? *Geophysical Research Letters*, *38*, L16704. https://doi.org/10.1029/2011GL048237

Kug, J. S., Jin, F. -F., & An, S. -I. (2009). Two types of El Niño events: Cold tongue El Niño and warm pool El Niño. *Journal of Climate*, *22*(6), 1499–1515. https://doi.org/10.1175/2008JCLI2624.1

Larkin, N. K., & Harrison, D. (2002). ENSO warm (El Niño) and cold (La Niña) event life cycles: Ocean surface anomaly patterns, their symmetries, asymmetries, and implications. *Journal of Climate*, *15*(10), 1118–1140. https://doi.org/10.1175/1520-0442(2002)015<1118:EWENOA>2.0.CO;2

Lee, T., Fukumori, I., & Tang, B. (2004). Temperature advection: Internal versus external processes. *Journal of Physical Oceanography*, *34*(8), 1936–1944. https://doi.org/10.1175/1520-0485(2004)034<1936:TAIVEP>2.0.CO;2

Lee, T., & McPhaden, M. J. (2010). Increasing intensity of El Niño in the central-equatorial Pacific. *Geophysical Research Letters*, *37*, L14603. https://doi.org/10.1029/2010GL044007

Masumoto, Y., Sasaki, H., Kagimoto, T., Komori, N., Ishida, A., Sasai, Y., et al. (2004). A fifty-year eddy-resolving simulation of the world ocean—Preliminary outcomes of OFES (OGCM for the Earth simulator). *Journal of the Earth Simulator*, *1*, 35–56.

McGregor, S., Ramesh, N., Spence, P., England, M. H., McPhaden, M. J., & Santoso, A. (2013). Meridional movement of wind anomalies during ENSO events and their role in event termination. *Geophysical Research Letters*, *40*, 749–754. https://doi.org/10.1002/grl.50136

McPhaden, M. J. (2012). A 21st century shift in the relationship between ENSO SST and warm water volume anomalies. *Geophysical Research Letters*, *39*, L09706. https://doi.org/10.1029/2012GL051826

McPhaden, M. J., Zebiak, S. E., & Glantz, M. H. (2006). ENSO as an integrating concept in Earth science. *Science*, *314*(5806), 1740–1745. https://doi.org/10.1126/science.1132588

Meinen, C. S., & McPhaden, M. J. (2000). Observations of warm water volume changes in the equatorial Pacific and their relationship to El Niño and La Niña [J]. *Journal of Climate*, *15*(20), 3551–3559.

Monahan, A. H., & Dai, A. (2004). The spatial and temporal structure of ENSO nonlinearity. *Journal of Climate*, *17*(15), 3026–3036. https://doi.org/10.1175/1520-0442(2004)017<3026:TSATSO>2.0.CO;2

Neske, S., & McGregor, S. (2018). Understanding the warm water volume precursor of ENSO events and its interdecadal variation. *Geophysical Research Letters*, *45*. https://doi.org/ 10.1002/2017GL076439

Okumura, Y. M., & Deser, C. (2010). Asymmetry in the duration of El Niño and La Niña. *Journal of Climate*, *23*(21), 5826–5843. https://doi.org/10.1175/2010JCLI3592.1

Ren, H., & Jin, F. (2013). Recharge oscillator mechanisms in two types of ENSO. *Journal of Climate*, *26*(17), 6506–6523. https://doi.org/10.1175/JCLI-D-12-00601.1

Rodgers, K. B., Friederichs, P., & Latif, M. (2004). Tropical Pacific decadal variability and its relation to decadal modulations of ENSO. *Journal of Climate*, *17*(19), 3761–3774. https://doi.org/10.1175/1520-0442(2004)017<3761:TPDVAI>2.0.CO;2

Santoso, A., McPhaden, M. J., & Cai, W. (2017). The defining characteristics of ENSO extremes and the strong 2015/2016 El Niño. *Reviews of Geophysics*, *55*, 1079–1129. https://doi.org/10.1002/2017RG000560

Santoso, A., Sen Gupta, A., & England, M. H. (2010). Genesis of Indian Ocean mixed layer temperature anomalies: A heat budget analysis. *Journal of Climate*, *23*(20), 5375–5403. https://doi.org/10.1175/2010JCLI3072.1

Su, J., Zhang, R., Li, T., Rong, X., Kug, J.-S., & Hong, C.-C. (2010). Causes of the El Niño and La Niña amplitude asymmetry in the equatorial eastern Pacific. *Journal of Climate*, *23*(3), 605–617. https://doi.org/10.1175/2009JCLI2894.1

Timmermann, A., An, S. I., Kug, J. S., Jin, F. F., Cai, W., Capotondi, A., et al. (2018). El Niño-Southern Oscillation complexity. *Nature*, *559*(7715), 535–545. https://doi.org/10.1038/s41586-018-0252-6

Walters, R. A., & Heston, C. (1982). Removing tidal-period variations from time-series data using low-pass digital filters. *Journal of Physical Oceanography*, *12*(1), 112–112, 115. https://doi.org/10.1175/1520-0485(1982)012<0112:RTPVFT>2.0.CO;2

Wang, W., & McPhaden, M. J. (2001). Surface layer temperature balance in the equatorial Pacific during the 1997–98 El Niño and 1998-99 La Niña. *Journal of Climate*, *14*(16), 3393–3407. https://doi.org/10.1175/1520-0442(2001)014<3393:SLTBIT>2.0.CO;2

Wen, C., Kumar, A., Xue, Y., & McPhaden, M. J. (2014). Changes in tropical Pacific thermocline depth and their relationship to ENSO after 1999. *Journal of Climate*, *27*(19), 7230–7249. https://doi.org/10.1175/JCLI-D-13-00518.1

Xiang, B., Wang, B., & Li, T. (2013). A new paradigm for the predominance of standing central Pacific warming after the late 1990s. *Climate Dynamics*, *41*(2), 327–340. https://doi.org/10.1007/s00382-012-1427-8

Zhang, X. B., & McPhaden, M. J. (2010). Surface layer heat balance in the eastern equatorial Pacific Ocean on interannual time scales: Influence of local versus remote wind forcing. *Journal of Climate*, *23*(16), 4375–4394. https://doi.org/10.1175/2010JCLI3469.1